Journal of Applied Electrochemistry (2005) 35:437–443
DOI 10.1007/s10800-005-0292-0

Electrochemical kinetic behaviour of the aqueous manganese dioxide electrode

GREGORY J. BROWNING and SCOTT W. DONNE*
Discipline of Chemistry, University of Newcastle, Callaghan, NSW, 2308, Australia
*(*author for correspondence, e-mail: scott.donne@newcastle.edu.au; phone: +61-(2)-4921-5477; fax: +61-(2)-4921-5472)*

Received 31 August 2004; accepted in revised form 10 December 2004

Key words: constant current discharge, electrochemical kinetics, EMD, manganese dioxide

Abstract

The processes involved in the reduction of an electrolytic manganese dioxide (EMD) were investigated and their exchange current densities were determined. The dQ/dE vs E curve was fitted by least squares minimisation with peaks based on the Nernst equation. The derivation of the peak model is described. In the potential range of 0.3 to −0.4 V (vs Hg/HgO reference), nine processes were found to contribute to the overall reduction. Exchange current densities for three of the main processes were determined from the movement of the deconvoluted peaks during a series of constant current discharge experiments.

1. Introduction

In today's society, portability is the key to the functionality and popularity of electronic devices. Power sources for these devices are almost exclusively batteries, of which those based on the aqueous Zn/MnO_2 system represent a significant proportion of the total battery market, due mainly to the performance characteristics of the manganese dioxide cathode. Despite this popularity, very little fundamental electrochemical information is know about its behaviour. The reasons for this are due in part to the complexity of the system, in particular the interplay between material structure and electrochemical behaviour.

The preferred manganese dioxide structure for aqueous electrochemical applications is the γ form, which is believed to be based on a molecular level intergrowth between pyrolusite (β-MnO_2) and ramsdellite, as shown in Figure 1 [1]. The basic building block for these structures is the [MnO_6] octahedra, which arranges itself in either edge- or corner-sharing modes to form the various tunnel (as in this case) or layered structures [2]. For γ-MnO_2 (Figure 1c), the randomness of the pyrolusite and ramsdellite intergrowth contributes to overall structural disorder [1]. Other structural defects found inherent to γ-MnO_2 include cation vacancies (x), partially reduced species (y), and structural water derived from the presence of protons in the structure necessary for the positive charge deficiency caused by the previous two defects [3]. The resulting composition is:

$$(Mn^{4+})_{1-x-y}\cdot(\square)_x\cdot(Mn^{3+})_y\cdot(O^{2-})_{2-4x-y}\cdot(OH^-)_{4x+y} \quad (1)$$

where $\square$ represents a cation vacancy. A more recent development is the inclusion of microtwinning in the γ-MnO_2 structure [4]; however, there is still debate as to whether it physically exists [5].

With this physical picture of the γ-MnO_2 structure, we are now in the position to examine its electrochemical reduction. The current discharge model for power generation in aqueous alkaline manganese dioxide cathode is the "electron-proton" mechanism proposed originally by Kozawa et al. [6–11]. This is a homogeneous process covering the compositional range from $MnO_{2.0}$ to $MnO_{1.5}$ (MnOOH). As shown in Figure 2, this process involves electron insertion into the structure, via the conductive network (typically graphite), to reduce a Mn^{4+} ion to Mn^{3+}. The corresponding positive charge deficiency is compensated for by proton insertion as a result of water decomposition at the solid/electrolyte interface. It has been shown that from the onset of discharge to near completion, the electronic conductivity of γ-MnO_2 is higher than its proton conductivity [12]. As a result, there is a build up of reduced species (H^+/e^- pairs) at the solid/electrolyte interface that is removed by proton and electron hopping to adjacent suitable sites further away from the surface into the material bulk. The driving force for this diffusion is the proton and electron activity gradient between the surface and bulk manganese dioxide, and it is believed to be discharge rate limiting. In other words, at high discharge rates, the rate of reduction is faster than the rate at which reduced species can be removed from the solid/electrolyte interface. Under these circumstances the surface becomes prematurely saturated with protons and electrons causing the electrode potential to

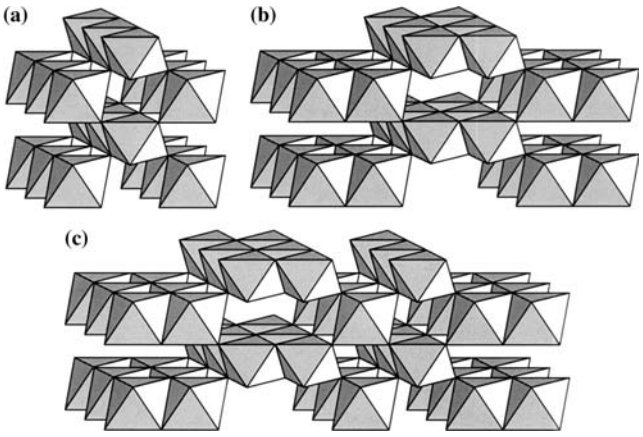

Fig. 1. Crystal structures of (a) pyrolusite, (b) ramsdellite, and (c) γ-MnO_2.

drop to values too low to be useful before all of the available capacity can be extracted.

The microscopic structure of γ-MnO_2 influences the diffusion rate of reduced species away from the surface. In particular, the (1×2) tunnels in ramsdellite (Figure 1b) have been shown through first principles calculations to be ideally suited to proton hopping and hence mass transport [13]. For other tunnel sizes, the proton hopping distance is too large thus restricting mass transport. A number of experimental works have also identified a series of energetically distinct steps during homogeneous reduction [4, 14–19]. Swinkels et al. [14] identified three processes during homogeneous reduction which they attributed to the reduction of ramsdellite domains, pyrolusite domains, and Mn^{4+} species on the boundaries between the two. Chabre and Pannetier [4] also identified three processes, but attributed the third process to reduction of the surface sites on the MnO_2 particle. These authors also observed a double peak in the region assigned to ramsdellite reduction, attributable to the successive insertion of protons into the two possible sites in the (1×2) channels of the ramsdellite structure.

The exchange current density is an important parameter in the characterization of any electrochemical system. It is essentially the maximum current able to be drawn from the electrode before deviation from the equilibrium potential occurs. The authors are not aware of any published studies where the exchange current density for γ-MnO_2 has been reported.

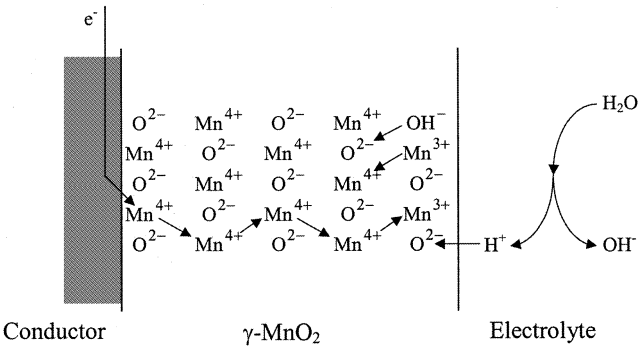

Fig. 2. Schematic diagram of proton and electron movements during discharge.

Previously, a potential sweep method was used to determine characteristic sweep rates (analogous to an exchange current density) for an electrochemical process. Angerstein-Kozlowska and Conway [20] determined the characteristic sweep rate for the adsorption of hydrogen on platinum by observing the change in voltammogram peak position with different sweep rates. A theoretical analysis of the potential sweep method was given by Srinivasan and Gileadi [21]. In a series of similar cyclic voltammetry experiments on $Mn(OH)_2$ in alkaline media, Cha and Park [22] observed peak movement with different scan rates. However, the characteristic scan rate or exchange current density for the electrochemical processes were not quantified.

In this work we will report on a novel way of interpreting chronopotentiometric discharge data generated for the manganese dioxide electrode. The method involves deconvoluting the electrochemical data into energetically different processes and then examining how their voltage changes as a function of discharge rate. As experiments are performed under constant current conditions, the exchange current density can be determined directly. The end result is an interpretation of electrochemical kinetic behaviour over the entire discharge range.

2. Experimental

2.1. *Sample preparation*

The starting material in this work was a commercial electrolytic manganese dioxide (EMD) provided by Delta EMD Australia, Proprietary Ltd. It was prepared by electrolysis of a hot (~98°C), acidic solution of $MnSO_4$ (acid to Mn ratio ~0.3), resulting in deposition of the EMD onto a titanium anode. Following deposition, the EMD was mechanically removed from the anode, milled to form a −105 μm powder, neutralized and washed to remove any entrained electrolyte, and then dried before being ready for use.

The working electrode was prepared by mixing thoroughly the manganese dioxide sample (0.200 g), Timcal SFG6 graphite (2.000 g) and 9 M KOH (0.370 g) using a mortar and pestle. After this the mixture was stored in an airtight container overnight to equilibrate before being used.

2.2. *Electrochemical cell preparation*

The cell used is shown schematically in Figure 3. Cell assembly involved placing the amount of sample mixture corresponding to 0.020 g of manganese dioxide into a Teflon-lined C-size battery can. The sides of the Teflon sleeve were brushed down to remove attached particles and three separator papers were placed on top of the sample. A stainless steel piston was then inserted into the can and used to compress the sample mixture (under

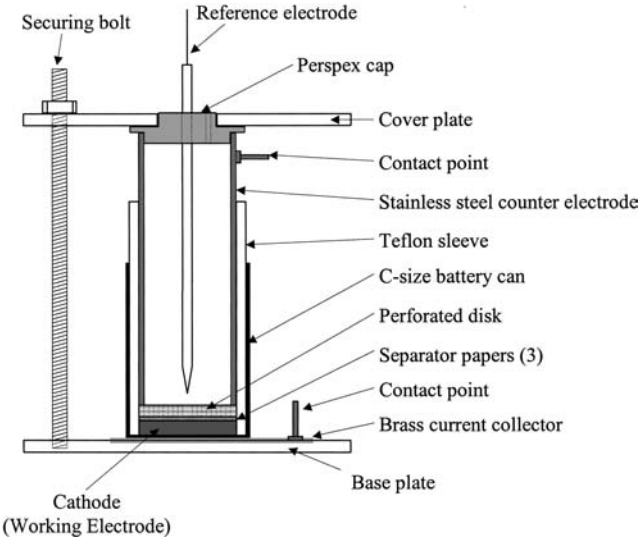

Fig. 3. Schematic diagram of the electrochemical cell.

1 tonne) to form a compact electrode within the cell. After compaction, the piston was removed and replaced with a perforated Perspex separator disc and a cylindrical stainless steel counter electrode. The chamber was then filled with ~15 mL of 9 M KOH electrolyte and the Perspex cap inserted. The cell was then mounted between the cover and baseplate, on top of the brass current collector, and held in place with three securing bolts each tightened to a torque of 0.75 Nm to ensure a uniform pressure. A Hg/HgO reference electrode was inserted into the completed cell, which was then left to equilibrate for one hour prior to discharge.

2.3. *Discharge regime*

To determine the starting potential for the experiment, the open circuit voltage (OCV) of the EMD needed to be determined. A small amount of EMD was added to 9 M KOH solution, shaken and allowed to settle and equilibrate for 24 hours. The OCV was measured across a platinum disk electrode placed on the surface of the EMD and a Hg/HgO reference electrode in the solution.

Cell discharge was controlled using a Perkin–Elmer Instruments VMP multi-channel potentiostat. To remove the effect of surface reduction of the EMD by the graphite, the sample mixture was initially re-oxidised to the OCV of the EMD using a 6 mA anodic current. The cell was equilibrated at this potential, after which it was reduced by constant current to −0.75 V (vs Hg/HgO). A series of experiments was performed using currents ranging from 0.02–6 mA (0.01–0.3 Ag^{-1} of EMD).

3. Results and discussion

3.1. *Deconvolution of electrochemical processes*

The reduction of γ-MnO_2 can be described by the expression

$$MnOOH_r + \Delta H_2O + \Delta e^- \rightarrow MnOOH_{r+\Delta} + \Delta OH^- \quad (2)$$

where r and Δ are the mole fractions of hydrogen in the γ-MnO_2 structure before and after reduction, respectively. Typically r lies in the range $0.1 < r < 0.9$, during which a solid solution of protons and electrons are formed in the structure. In an undischarged material $r \approx 0.1$, and when $r > \sim 0.9$ structural rearrangement occurs to form a distinct MnOOH phase. There is experimental evidence to suggest that there are energetically different domains within the γ-MnO_2 structure [4, 14–19]. Equation (2) suggests that the γ-MnO_2 structure can be partially reduced and that Mn^{3+} and Mn^{4+} ions can coexist in the structure. The electrode potential for the reduction described in Equation (2) is given by the corresponding Nernst equation; *i.e.*,

$$E = E^{o'} + \frac{RT}{nF}\ln\left(\frac{a(MnOOH_r)\cdot a(H_2O)^{\Delta}}{a(MnOOH_{r+\Delta})\cdot a(OH^-)^{\Delta}}\right) \quad (3)$$

where $E^{o'}$ is the standard reduction potential, n is the stoichiometric number of electrons involved in the charge transfer reaction, a(X) is the activity of species X, and the remaining symbols have their usual significance. Under the discharge conditions used, $a(H_2O)$ and $a(OH^-)$ are essentially constant. Therefore,

$$E = E^{o} + \frac{RT}{nF}\ln\left(\frac{a(MnOOH_r)}{a(MnOOH_{r+\Delta})}\right) \quad (4)$$

where E^{o} takes into consideration the contributions to the potential from $a(H_2O)$ and $a(OH^-)$. Let us now assume that the activities in Equation (4) can be approximated by mole fractions; *i.e.*,

$$E = E^{o} + \frac{RT}{nF}\ln\left(\frac{X(MnOOH_r)}{X(MnOOH_{r+\Delta})}\right) \quad (5)$$

From this equation, the terms $X(MnOOH_r)$ and $X(MnOOH_{r+\Delta})$ represent essentially the mole fractions of Mn^{4+} and Mn^{3+} in a particular domain within the structure; *i.e.*,

$$E = E^{o} + \frac{RT}{nF}\ln\left(\frac{X(Mn^{4+})}{X(Mn^{3+})}\right) \quad (6)$$

where X is the mole fraction of the Mn^{4+} and Mn^{3+} species. Assuming all the manganese is initially in the 4+ state, the number of moles of Mn^{3+} formed can be determined from the charge, Q, using

$$\text{moles of } Mn^{3+} = \frac{Q}{nF} \quad (7)$$

The number of moles of Mn^{4+} remaining is given by

$$\text{moles of } Mn^{3+} = M - \frac{Q}{nF} \tag{8}$$

where M is the total number of moles of manganese species. By substituting Equation (7) and (8), Equation (6) becomes

$$E = E^{o} + \frac{RT}{nF}\ln\left(\frac{nMF - Q}{Q}\right) \tag{9}$$

Equation (9) can be rearranged in terms of Q

$$Q = \frac{nMF}{1 + \exp\left(\frac{nF}{RT}(E - E^{o})\right)} \tag{10}$$

By differentiating Equation (10) with respect to E, an expression that describes the discharge process is produced; *i.e.*,

$$\frac{dQ}{dE} = \frac{-\frac{n^2MF^2}{RT}\exp\left(\frac{nF}{RT}(E - E^{o})\right)}{1 + \exp\left(\frac{nF}{RT}(E - E^{o})\right)} \tag{11}$$

The minus sign in Equation (11) is indicative of a reduction process. With this expression, voltammetric or galvanostatic data that is expressed as dQ/dE versus E can be modelled with n, M and E^{o} as variables.

Before proceeding to use Equation (11), it is important that the assumptions made in its derivation be discussed. They include:

(i) The first assumption was that H_2O and OH^- activities remained constant throughout discharge. All discharge experiments used a flooded test cell so that electrolyte availability would not be a limiting factor during discharge. The excess of electrolyte ensures that its concentration does not change significantly during discharge, and therefore the activities of OH^- and H_2O also do not change significantly.

(ii) The next assumption was that the activities of $MnOOH_r$ and $MnOOH_{r+\Delta}$ could be represented by mole fractions. An assumption like this had to be made since there is very little data available on activity coefficients of species in the γ-MnO_2 structure. The validity of this assumption is not known at this time. Another alternative to activities is to use molar concentrations in the Nernst equation. This assumption was not made because using concentrations introduces a volumetric term. The structure of γ-MnO_2 is known to expand during reduction and so the dependency of concentration on volume introduces added complexity.

(iii) It was also assumed that the mole fractions of $MnOOH_r$ and $MnOOH_{r+\Delta}$ could be represented by the mole fractions of Mn^{4+} and Mn^{3+} within the structure, respectively. This is a reasonable assumption since Mn^{4+} and Mn^{3+} are the electroactive species within the structure and their mole ratio is directly related to electrode potential.

(iv) Another assumption was that the potential predicted by the Nernst equation is equivalent to the operating voltage of the manganese dioxide electrode; *i.e.*, there is no electrode polarization during discharge. This assumption can only be true if there is negligible resistance to charge transfer, and also that diffusion limitations are negligible. To satisfy these criteria all electrodes were prepared with a high proportion of graphite so that electronic transport within the cathode was not limiting. Furthermore, electrodes were discharged under flooded conditions so that ionic transport within the cathode was not limiting.

(v) Another very important assumption is that the reduction processes are indeed all occurring in the solid state. Previous work in concentrated alkaline electrolytes [18] has demonstrated that dissolution of the manganese dioxide electrode occurs at high depths of discharge (low voltages) approaching heterogeneous reduction. In this work our interest is in understanding the higher voltage processes, which are most important for power generation, and where experiments have shown reduction to be solely in the solid state.

The fact that the manganese dioxide electrode is dependent on solid state diffusion leaves this as the main limitation to performance, and hence the feature to be characterized in this work. Furthermore, since proton transport in γ-MnO_2 is diffusion limiting for the majority of discharge, it is the specific material property under study. In traditional solution-based electrochemical experiments, it is typical to reach a situation where the measured response is diffusion limited; *e.g.*, the diffusion limited current in polarography. The amount of material taking part in the electrochemical reaction is also much less in solution-based electrochemistry; *i.e.*, the electroactive species within the diffusion layer. This is a completely different situation to the manganese dioxide electrode, and solid state electrodes in general, in which case all of the electroactive material can be reduced or oxidized.

The effects of n, M and E^{o} on dQ/dE are shown in Figure 4. During the derivation of Equation (11), n was assumed to represent the stoichiometric number of electrons involved in the electrochemical process. However, as shown in Figure 3a, n can be more properly regarded as an indicator of the facility of the electrochemical reduction. For instance, processes that are kinetically very fast would tend to be reduced over a very narrow potential range, hence giving a sharp dQ/dE peak. Conversely, a sluggish electrochemical process would be expected to cover a large potential range, thus leading to a flat dQ/dE peak. The value of M indicates the number of moles of species associated with the corresponding dQ/dE peak. From a plot of dQ/dE versus E, the integrated area under the peak can also be converted to M. Finally, as expected, E^{o} is an indicator of the potential of the peak maxima.

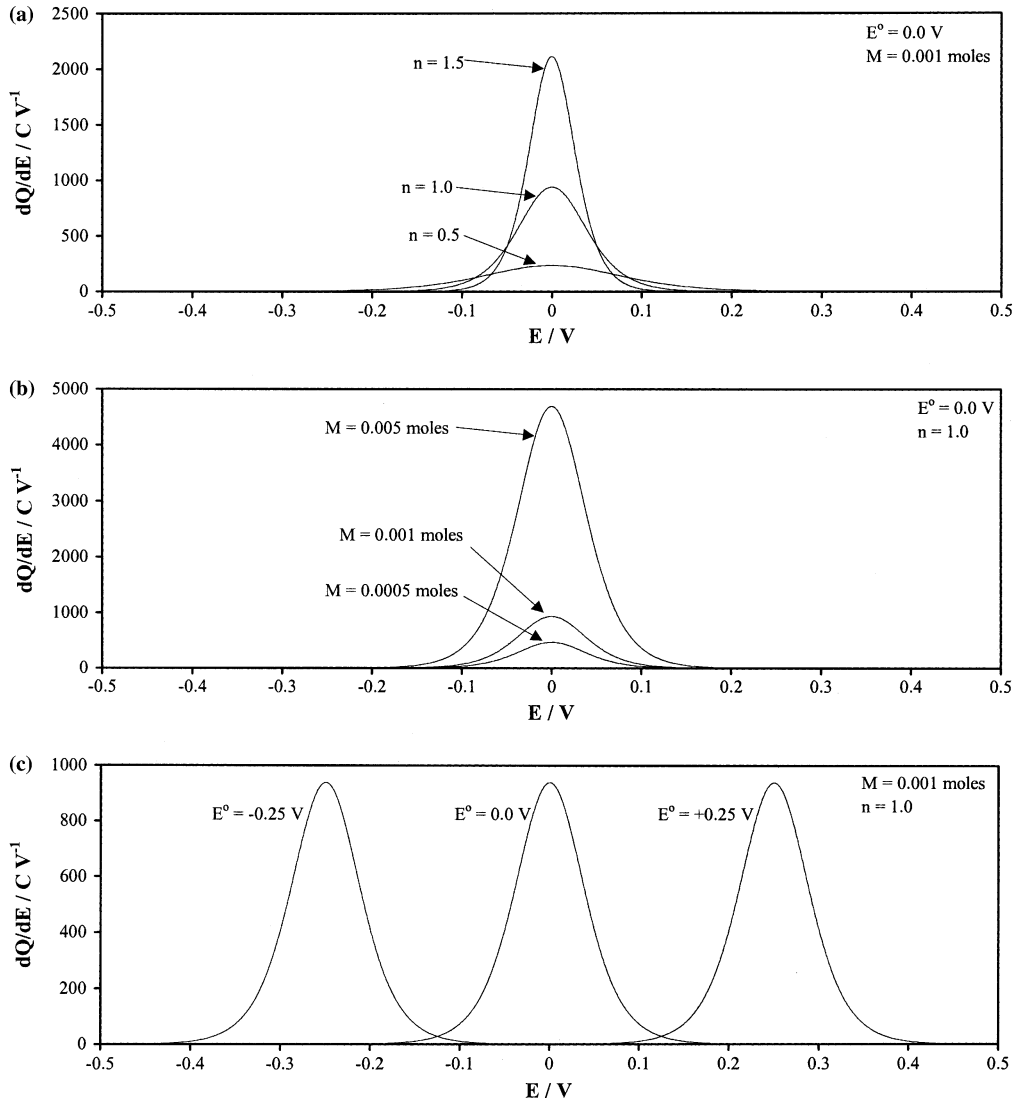

Fig. 4. Effect of (a) n, (b) M, and (c) E^o on electrochemical behaviour.

3.2. *Discharge results*

The results obtained from these discharge experiments were in the form of potential as a function of time. Since the current (i) is constant throughout each test, the charge through the cell (Q) is proportional to time (t); *i.e.*,

$$Q = it \tag{12}$$

From this a plot of charge versus potential was generated (Figure 5a) and the derivative of this curve was calculated to produce a plot of dQ/dE vs E (Figure 5b). This plot clearly shows how discharge varies with changes in potential and, with deconvolution, allows the contributions of the various processes to be determined.

The ohmic resistance in the cell will cause a small difference between the measured potential and the potential experience by the sample. As such, a correction to the position of the peaks is needed. The resistance of each cell was measured using electrochemical impedance spectroscopy to be $\sim$0.65 Ω over the entire discharge [23]. Using Ohm's law, the potential drop due ohmic resistance was calculated from the discharge current and subtracted from peak potentials. As the resistance in the cell was low, the difference to the potential was negligible.

A series of eleven discharge experiments were performed at various currents ranging from 0.01 to 0.3 Ag^{-1} of EMD. Figure 6 shows the dQ/dE versus E plots for all discharge currents. It can be seen that as the discharge current was increased, a progressive change in the curves was produced. The peak height, and consequently the area under the curve, is reduced with increasing current. This indicates that at higher currents, not all of the Mn^{4+} is being utilised in the process. This plot also shows the potential at which the peak maxima occur moves to more negative values as discharge current is increased.

Under the discharge regime used in these experiments, the current was controlled in order to maintain a constant reaction rate. At low discharge currents, the kinetics of the reaction are fast relative to the controlled rate which enables the system to maintain equilibrium.

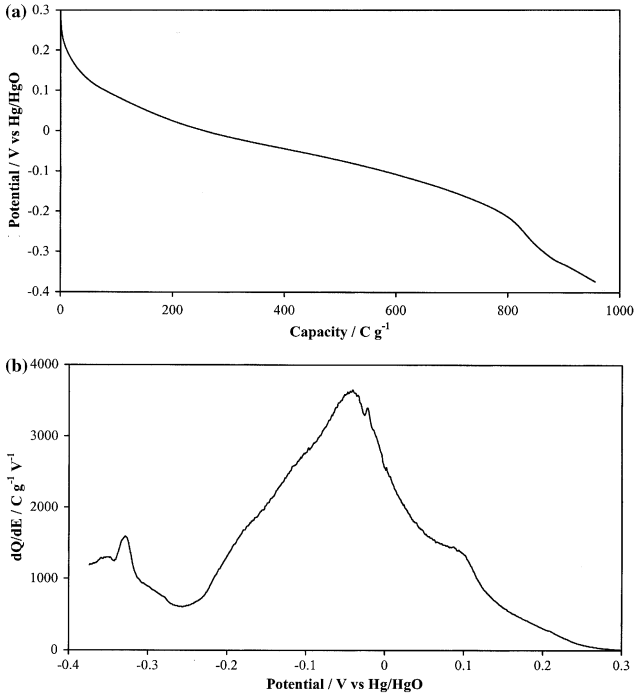

Fig. 5. Typical example of electrochemical data. (a) Q vs E, and (b) dQ/dE vs E.

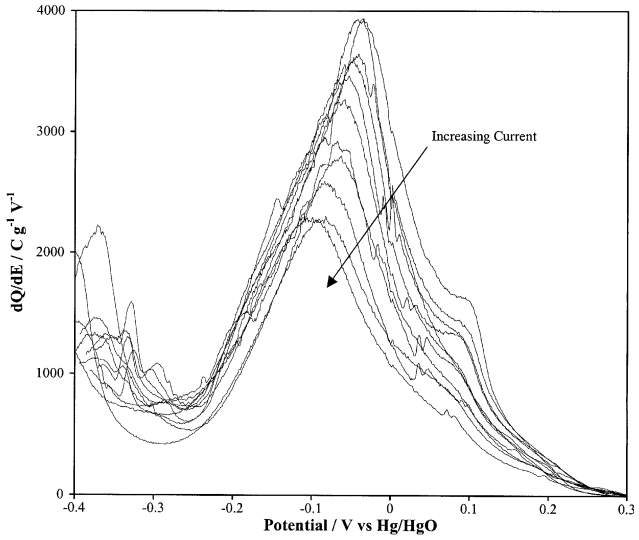

Fig. 6. Variation in dQ/dE with discharge current.

This results in peak maxima for each process to occuring at their standard reduction potential. However at high currents, reaction kinetics are slow relative to the forced reaction rate. The consequence of this is that the electrode potential shifts to more negative values in order to maintain the current.

The deconvolution of each of the dQ/dE vs E plots was performed by least squares minimisation, using peaks of the form described in Equation (11). An example of the resultant curves is presented in Figure 7. It shows that over the potential range of 0.3 to −0.4 V, the dQ/dE vs E curve consists of nine peaks, each as a

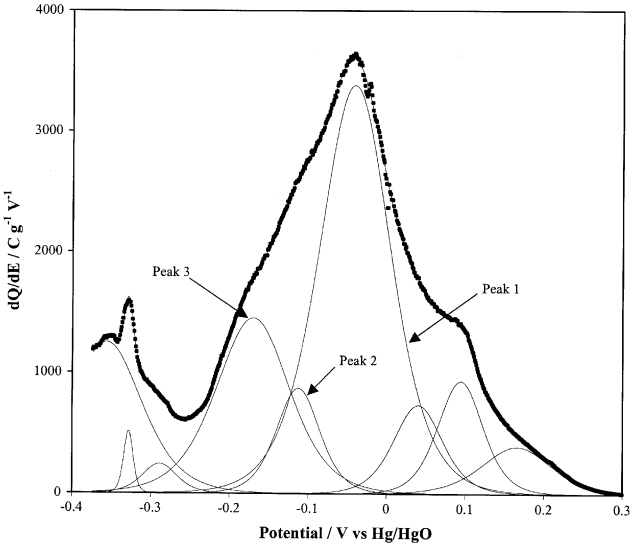

Fig. 7. dQ/dE vs E showing component peaks.

result of a different reduction process. It is thought that each of these peaks is due to reduction of Mn^{4+} ions in different structural domains. Previous studies [4, 14–19] have attempted to describe the discharge curve in terms of three regions corresponding to pyrolusite, ramsdellite and surface or boundary sites. Hong et al. [15] also observed a double peak in the region assigned to ramsdellite reduction. This was attributed to successive proton intercalation into the two sites in ramsdellite. With the presence of nine peaks occurring over the potential range studied in this work, the three-region description of the discharge is perhaps only adequate to describe the major reduction processes. Evidence to be able to identify all processes is sparse [5], as well as outside the scope of this paper, but nevertheless will be the subject of future work.

3.3. *Exchange current density*

The exchange current density corresponds to the maximum discharge current at which the electrode potential does not deviate from its equilibrium value. For practical applications, it is desirable to have as high an exchange current density as possible. This point can be determined from how peak positions change with discharge current. At discharge currents lower than the exchange current density, the positions of the peaks in the dQ/dE vs E plot remain constant. At higher currents, the peaks move to more negative potentials. Figure 8 shows a Tafel-type plot of the peak potential versus current on a logarithmic scale for the three main peaks indicated in Figure 7. At low currents, the peak potentials are relatively constant, corresponding to E^{o} for the process. At higher currents, the peak potentials shift linearly to more negative potentials with current. The point at which there is a change in the slopes of the lines corresponds to the exchange current density for that process.

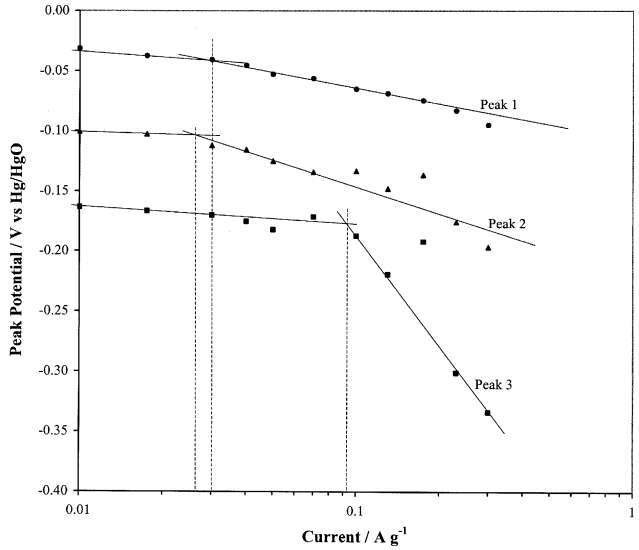

Fig. 8. Peak potential as a function of discharge current.

Figure 8 shows that for peaks 1 and 2 the exchange current density was $\sim$0.03 Ag^{-1}, and for peak 3 $\sim$0.095 Ag^{-1}.

4. Conclusions

During the reduction of γ-MnO_2, the number of energetically different processes occurring was found to be greater than previously reported. By deconvolution of the dQ/dE vs E curve, nine processes have been found in the potential range of 0.3 to -0.4 V (vs Hg/HgO reference). The identity of each of these processes is the subject of ongoing work.

A series of constant current discharge experiments were performed and the potential at which the peak maxima occur plotted as a function of log(i). At low currents, the peak potentials remained constant whereas at high currents, the peak potentials shifted to more negative values due to performance limitations. The current at which these limitations becomes negligible is the exchange current density and was found to be $\sim$0.03 Ag^{-1} for peaks 1 and 2 and $\sim$0.095 Ag^{-1} for peak 3.

Further work is required to identify the species in the EMD associated with the deconvoluted peaks and whether the exchange current densities are constant for EMD synthesised under different conditions.

Acknowledgements

The authors acknowledge financial support for this project by the Australian Research Council (LP0346943) and Delta EMD Australia Proprietary Ltd. Dr. Rodney Williams from Delta EMD is also acknowledged for many related technical discussions.

References

1. P.M. De Wolff, *Acta Cryst.* **12** (1959) 341.
2. Giovanoli R. (1980). *in* I.M. Varentsov, G. Grasselly (Eds), 'Geology and Geochemistry of Manganese, Vol. 1' (Akademiai Keadó, Budapest, 1980), pp 159–233.
3. P. Ruetschi, *J. Electrochem. Soc.* **131** (1984) 2737.
4. Y. Chabre and J. Pannetier, *Prog. Solid State Chem.* **23** (1995) 1.
5. A.H. Heuer, A.Q. He, P.J. Hughes and F.H. Feddrix, *ITE Letters on Batteries, New Technology and Medicine* **1** (2000) 926.
6. A. Kozawa and J.F. Yeager, *J. Electrochem. Soc.* **112** (1965) 959.
7. A. Kozawa, T. Kalnoki-Kis and J.F. Yeager, *ibid.* **113** (1966) 405.
8. A. Kozawa and R.A. Powers, *ibid.* **113** (1966) 870.
9. Idem, *Electrochem. Tech.* **5** (1967) 535.
10. Idem, *J. Electrochem. Soc.* **115** (1968) 122.
11. A. Kozawa and J.F. Yeager, *ibid.* **115** (1968) 1003.
12. X. Xi, L. Hong and C. Zhenhai, *ibid.* **136** (1989) 266.
13. D. Balachandran, D. Morgan, G. Ceder and A. wanevan de, *J. Solid State Chem.* **173** (2003) 2.
14. D.A.J. Swinkels, K.E. Anthony, P.M. Fredericks and P.R. Osbom, *J. Electroanal. Chem.* **168** (1984) 433.
15. Z. Hong, C. Zhenhai and X. Xi, *J. Electrochem. Soc.* **136** (1989) 2771.
16. S.W. Donne, G.A. Lawrance and D.A.J. Swinkels, *ibid.* **144** (1997) 2949.
17. Idem, *ibid.* **144** (1997) 2954.
18. Idem, *ibid.* **144** (1997) 2961.
19. Y. Paik, W. Bowden, T. Richards, R. Sirotina and C. Grey, *ibid.* **151** (2004) A998.
20. H. Angerstein-Kozlowska and B.E. Conway, *J. Electroanal. Chem.* **95** (1979) 1.
21. S. Srinivasan and E. Gileadi, *Electrochim. Acta* **11** (1966) 321.
22. D.K. Cha and S.M. Park, *J. Electrochem. Soc.* **144** (1997) 2573.
23. J.P. Arnott and S.W. Donne, Unpublished results.